# Indoor Localization Based on Floor Plans and Power Maps: Non-Line of Sight to Virtual Line of Sight

Joe J. Khalifeh and Zaher M. Kassas
*University of California, Riverside*
Samer S. Saab
*Lebanese American University*

## BIOGRAPHIES

Joe J. Khalifeh is a Ph.D. student at The University of California, Riverside. He received a B.E. in electrical engineering and an M.S. in computer engineering from the Lebanese American University (LAU). From 2012 to 2015, he was a research assistant at LAU. His research interests include navigation, autonomous vehicles, and intelligent transportation systems.

Zaher (Zak) M. Kassas is an assistant professor at The University of California, Riverside. He received a B.E. in Electrical Engineering from The Lebanese American University, an M.S. in Electrical and Computer Engineering from The Ohio State University, and an M.S.E. in Aerospace Engineering and a Ph.D. in Electrical and Computer Engineering from The University of Texas at Austin. From 2004 through 2010 he was a research and development engineer with the LabVIEW Control Design and Dynamical Systems Simulation Group at National Instruments Corp. His research interests include estimation, navigation, autonomous vehicles, and intelligent transportation systems.

Samer S. Saab is a Professor of electrical engineering and Associate Dean of the Department of Electrical and Computer Engineering at the Lebanese American University (LAU) in Byblos, Lebanon. He received the B.S., M.S., and Ph.D. degrees in electrical engineering and the M.A. degree in applied mathematics from the University of Pittsburgh, Pittsburgh, PA, in 1988, 1989, 1992, and 1990, respectively. From 1993 to 1996, he was with Union Switch and Signal and ABB Daimler-Benz Transportation, Pittsburgh. His research interests include iterative learning control, Kalman filtering, navigational positioning systems, and wireless communications.

## ABSTRACT

An indoor localization algorithm that is based on fingerprinting and trilateration is developed. The algorithm assumes *a priori* knowledge of the layout of the environment and the position of the transmitters. First, a power map is simulated around "strategically" sampled training points. Then, the power map is used to produce an initial estimate for the position of the receiver, from which the total losses due to obstacles in the environment are calculated. These losses are extracted from the received power, transforming the non line-of-sight environment to a virtual line-of-sight one. The position of the receiver is finally obtained from the distances estimated from the corrected power by an extended Kalman filter. Numerical simulations and experimental results are presented to evaluate the performance of the proposed algorithm.

## I. INTRODUCTION

Reliable and accurate indoor localization has considerable societal and economic impacts. The majority of emergency calls originate indoors on cell phones and many location-based services, such as people tracking, store locating, and proximity-based marketing, take place indoors. Several indoor localization technologies have been proposed, among the most promising of which are those exploiting ubiquitous wireless local area networks (WLAN or Wi-Fi) [1, 2]. Localization techniques can be broadly classified into triangulation/trilateration and fingerprinting.

Triangulation techniques are used to estimate the position of the receiver given the angle between the each transmitter and the main axis of the receiver's antenna. Trilateration methods are used to estimate the position of the receiver given the distances from the receiver to each of the transmitters. In order to compute distances and angles, methods such as time of arrival (TOA), time difference of arrival (TDOA), phase of arrival (POA), and angle of arrival (AOA) are used. Although such techniques could theoretically deliver centimeter-level accuracy, they are practically prohibitive indoors, since they require a complex receiver architecture and due to propagation effects, such as fading, shadowing, and multipath [2]. The implementation of triangulation and trilateration methods that rely on TOA, TDOA, POA and/or AOA is becoming more feasible with the development of smart phone technology, especially on the models equipped with inertial measurement units (IMU) [3, 4]. Recent work exploits the IMUs and the dual antenna transceivers on mobile devices to implement a synthetic aperture RADAR (SAR) [4]. The SAR allows for the AOA to be calculated, hence localizing the receiver with a submeter accuracy.

However, when the receiver is not equipped with enough



**Preprint of the 2015 ION GNSS+ Conference Tampa, FL, September 14–18, 2015**

sensors, other localization methods must be employed. Fingerprinting is a cheaper and simpler technique than triangulation and is derived from received signal strength (RSS) measurements. A power map of RSS in the environment is typically constructed offline either via numerical simulations or experimental sampling. Several empirical models have been used to generate the power maps, such as the COST model and the Motley-Keenan model [5, 6]. Lightweight models to simulate the power map were developed to eliminate the cumbersome training phase [5]. However, these approaches compromise accuracy for a higher computational speed. Other methods were proposed to improve the accuracy of lightweight models, however, extra overhead was introduced as the environment has to be clustered manually into smaller areas [6]. For more accurate fingerprinting positioning, the power map is generated by collecting several training points– or reference points, in the real environment. The accuracy is hence improved, but at the cost of a laborious training phase. In order to minimize the work in the training phase, methods such as crowdsourcing have been developed [7]. Such methods consist of expanding the power map by acquiring received power and position information of any user in the environment. Other approaches aimed at automating the map building process by integrating IMUs and radio frequency receivers on a mobile platform [8, 9]. Whether generated from an empirical model or from real data, a power map will consist of a set of RSS values associated with a corresponding set of $(x, y)$ coordinates in the space. In the online stage, the position of the object is estimated by choosing the $(x, y)$ coordinates that minimize the error between the measured RSS and the pre-mapped RSS values. To this end, several techniques have been proposed, such as probabilistic methods, K-nearest neighbor (kNN) [10], neural networks [11], support vector machine (SVM) [12], and smallest M-vertex polygon (SMP) [13]. Other methods employed modified versions of a Kalman filter (KF) to estimate the receiver position with fingerprinting [14, 15]. Their method however fails to account for the discontinuities caused by the obstacles in the indoor environments. In general, fingerprinting techniques perform relatively well and do not require complex or expensive receivers. While these techniques are practically implementable on underlying wireless infrastructure, they possess two major drawbacks: (i) building the power map can be very cumbersome and laborious and (ii) the map needs to be updated whenever changes in the environment occur [16]. Other map-building methods use geostatistics to predict RSS measurements in unobserved locations, which reduce the number of required RSS measurements in the map-building process. Such techniques perform at a meter-level accuracy [17].

In this work, an indoor positioning technique that combines trilateration and fingerprinting coupled with an extended Kalman filter (EKF) is presented. The core of this method relies on transforming a non-line of sight (NLOS) environment to a virtual line of sight (VLOS) one, then solving for the position using trilateration. To the knowledge of the authors, no such approach has been proposed in the literature.

The proposed localization system assumes *a priori* knowledge of the floor plan of the environment and the layout of the transmitting antennas. The system consists of two stages. First, a power map for the environment is generated offline based on the transmitted power of the transmitting antennas. A power map is then simulated around several power measurements sampled at the minimum number of locations required to describe the entire environment. During the online stage, RSS measurements are taken from each transmitter, and an initial estimate of the receiver location is determined by employing a power map-matching (MM) algorithm. This MM algorithm is adapted from a similar algorithm designed for GPS signal power in outdoor environments [18]. The initial position estimate is used to calculate the losses due to hard partitions. These losses are extracted from the RSS measurements and the power map is updated, converting the NLOS environment to a VLOS. Finally, an EKF is employed to estimate the position of the receiver based on the corrected received power and the initial MM solution. The proposed approach is tested numerically and experimentally.

The remainder of the paper is organized as follows. Section II describes the received power and distance models. Section III discusses the proposed VLOS positioning algorithm. Section IV presents the simulation and experimental results of both the map matching algorithm and the VLOS positioning algorithm. Concluding remarks are given in section V.

## II. MODEL DESCRIPTION

In most applications, the receiver is only sensing the received signal power from the transmitter. A distance or range estimate has to be extracted from the measured power in order for the receiver to localize itself. Therefore, a model that relates the received power to the distance must be assumed. The proposed power and distance models are described in this subsection.

### A. Received Power Model

To model the radio frequency (RF) propagation in indoor environments, the log-distance path loss model will

be adopted [19], which is is given by

$$P_r(d) = P_0 - 10\,n\,\log_{10}\left(\frac{d}{d_0}\right) + w, \tag{1}$$

where $P_r(d)$ is the received power in dBm at a distance $d$ in meters, $P_0$ is the power received in dBm at the reference distance $d_0$, $n$ is the path loss exponent, and $w$ is a term that captures the effect of random shadowing, which is modeled as a zero-mean Gaussian random variable with variance $\sigma_w^2$. The values of $n$ and $\sigma_w$ depend on the frequency of the RF signal and on the layout of the indoor environment. Based on empirical studies, $n$ usually ranges between 2 and 3, and $\sigma_w$ is usually greater than a few dBs in indoor environments [19]. Such values of $n$ and $\sigma_w$ will introduce significant errors in the estimated range, which will in turn deteriorate the accuracy of the position solution. A more elaborate model, proposed by Motley-Keenan, takes into consideration the losses due to wall and floor partitions in the building, which yields a better estimate of the distance separating the transmitter and the receiver [5]. These losses can be estimated if the geometry of the environment is known (e.g., from blueprints). The Motley-Keenan model is given by

$$P_r(d) = P_0 - 10\,n\,\log_{10}\left(\frac{d}{d_0}\right) + N_w F_w + N_f F_f, \tag{2}$$

where $N_w$ and $N_f$ are the number of walls and the number of floors, respectively, separating the transmitter and the receiver and $F_w$ and $F_f$ are the average wall and floor attenuation factors, respectively. We propose a more elaborate model that considers the attenuation of each separate wall or floor individually. In the case of multiple transmitters, the model can be expressed as

$$P_r^{(j)}(d) = P_0^{(j)} - 10\,n\,\log_{10}\left(\frac{d^{(j)}}{d_0^{(j)}}\right) + \sum_{i=1}^{N_w} F_{w_i}^{(j)} + \sum_{q=1}^{N_f} F_{f_q}^{(j)}, \tag{3}$$

where $j \in \{1, 2, 3, ..., N_T\}$, $N_T$ is the total number of transmitters, $F_{w_i}$ and $F_{f_q}$ are the attenuation factors associated with wall $i$ and floor $q$, respectively. In real applications, the antenna of the transmitter is usually directional and therefore additional losses due to the azimuth and elevation angles are introduced. To account for these losses, (3) is modified to

$$P_r^{(j)}(d, \phi, \theta) \triangleq P_{r_0}^{(j)}(d) + L_p^{(j)} + L_D^{(j)}(\phi, \theta), \tag{4}$$

where $P_{r_0}^{(j)}(d) = P_0^{(j)} - 10\,n\,\log_{10}\left(\frac{d^{(j)}}{d_0^{(j)}}\right)$ is the power received when the receiver is at a distance $d^{(j)}$ in the line of sight (LOS) of the transmitter, $L_p^{(j)} \triangleq \sum_{i=1}^{N_w} F_{w_i}^{(j)} + \sum_{q=1}^{N_f} F_{f_q}^{(j)}$ are the total losses due to the wall and floor partitions obstructing the transmitter, and $L_D^{(j)}(\phi, \theta)$ are the losses due to the elevation angle $\theta$ and the azimuth angle $\phi$. In the sequel, the superscript $(j)$ will be dropped for simplicity of notation. $L_D(\phi, \theta)$ can be deduced from the radiation pattern of the antenna, which is usually provided by the manufacturer. For example, Fig. 1 shows the radiation patterns for the antenna of the CISCO 3700i Access Point (AP) that are used in the experiments for this work [20].

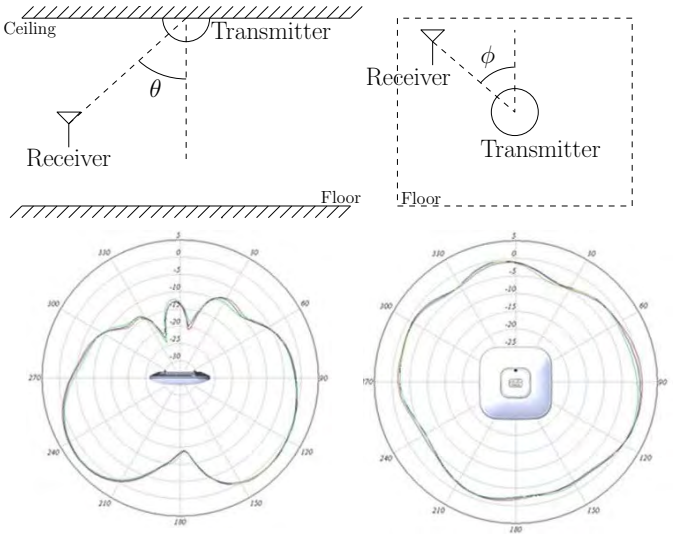


Fig. 1. Elevation angle $\theta$ (top left), azimuth angle $\phi$ (top right), radiation pattern in the elevation angle plane (bottom left), and radiation pattern in the azimuth angle plane (bottom right).

With the knowledge of the partition losses and the radiation pattern of the antenna, the received power can be corrected in order to estimate the distance to the transmitter more accurately. The corrected received power $\bar{P}_r(d)$ is given by

$$\begin{aligned}\bar{P}_r(d) &= P_r(d, \phi, \theta) - L_p - L_D(\phi, \theta) \\ &= P_0 - 10\,n\,\log_{10}\left(\frac{d}{d_0}\right).\end{aligned} \tag{5}$$

It can be seen from (5) that $\bar{P}_r(d)$ is equal to the received power at a distance $d$ in the LOS of the transmitter. The partitioned environment can therefore be transformed into a VLOS environment, where the apparent received power, called VLOS power, is given by $\bar{P}_r(d)$. Using the VLOS power to estimate the distance to the transmitter yields more accurate distance estimates, and subsequently a more accurate position solution. However, obtaining $\bar{P}_r(d)$ requires the knowledge of $L_p$ and $L_D(\phi, \theta)$, which in turn depend on the position of the receiver. To resolve this issue, a fingerprinting-based approach to produce an initial estimate for the receiver's position is developed in Section III. The initial position estimate of the receiver is then used to calculate $L_p$, $L_D(\phi, \theta)$, and the VLOS power.

### B. Distance Model

Although the employed VLOS model accounts for partition and angle losses, other fluctuations in power occur due

to multipath, receiver sensitivity, radiation pattern accuracy, and wall and floor attenuation factors accuracy [19]. These fluctuations are modeled as a zero-mean Gaussian random variable. To account for these fluctuations, (5) is adjusted as

$$\bar{P}_r(d) = P_0 - 10\,n\,\log_{10}\left(\frac{d}{d_0}\right) + \upsilon,$$

where $\upsilon$ is a zero-mean Gaussian random variable with variance $\sigma^2$. While $\sigma^2$ is smaller than $\sigma_w^2$– variance of the noise term $w$ in (1), $\upsilon$ can significantly affect the accuracy of the estimated distance, since it enters the distance estimate through the relationship

$$\bar{d} \cong d_0 10^{\frac{P_0 - \bar{P}_r(d) + \upsilon}{10n}}.$$

The error introduced by $\upsilon$ to $\bar{d}$ is captured through the relationship

$$\bar{d} = d + \delta d_\sigma(d),$$

where $\delta d_\sigma(d)$ is the distance error resulting from the noise $\upsilon$. The mean $\eta$ and variance $r$ of $\delta d_\sigma(d)$ can be shown to be

$$\begin{aligned} \eta(d) &= d(\gamma - 1) \\ r(d) &= d^2\gamma^2(\gamma^2 - 1), \end{aligned} \tag{6}$$

where $\gamma \triangleq \exp\left(\frac{1}{2}\left[\frac{\ln(10)\sigma}{10n}\right]^2\right)$. Therefore, at any time instant $k$, the vector of observed distances from all the different transmitters can be expressed as

$$\bar{\boldsymbol{d}}(k) = \boldsymbol{d}(k) + \Delta\boldsymbol{d_\sigma}(k), \tag{7}$$

where $\bar{\boldsymbol{d}}(k) = [\bar{d}^{(1)}(k), ..., \bar{d}^{(N_T)}(k)]^T$ is a vector of observed distances from all the different transmitters, $\boldsymbol{d}(k) = [d^{(1)}(k), ..., d^{(N_T)}(k)]^T$ is a vector of the true distances from all the different transmitters, and $\Delta\boldsymbol{d_\sigma}(k) = [\delta {d_\sigma}^{(1)}(k), ..., \delta {d_\sigma}^{(N_T)}(k)]^T$ is a vector of independent measurement noise associated with the distance from each of the transmitters, with $\boldsymbol{\eta}(d) = [\eta^{(1)}(k), ..., \eta^{(N_T)}(k)]^T$, and covariance $\boldsymbol{R}(k) = \text{diag}\left[r^{(1)}(k), ...r^{(N_T)}(k)\right]$.

## III. VLOS POSITIONING ALGORITHM

The positioning algorithm proposed in this paper consists of two phases:

**(i) Map Building:** The received power map of the environment is generated off-line. The power map is used to obtain an initial estimate for the position of the receiver.

**(ii) VLOS Positioning:** An initial estimate of the receiver position is produced based on the received power measured online and on the previously generated power maps. The partition and angle losses at the initial position estimate are then calculated. Subsequently, the measured received power is corrected and the distance between the receiver and each of the transmitters is extracted and passed as an observation to an EKF, which estimates the receiver's position.

These phases are discussed in the following two subsections.

### A. Map Building Algorithm

In order to transform the environment into a VLOS one, the knowledge of $L_p$ and $L_D(\phi, \theta)$ is required. As mentioned earlier, the values of $L_p$ and $L_D(\phi, \theta)$ depend on the position of the receiver. A fingerprinting-based approach to obtain an initial estimate for the position of the receiver is proposed in this subsection.
Fingerprinting is the process of selecting a receiver position that maximizes the probability of the receiver being at the selected position, given a measured received power and a previously generated power map. Bayesian filters are usually employed to maximize this probability. The power map is built in a training or an off-line stage. Several power samples associated with different receiver positions are collected and stored in a database (or a map). Each pair of measured received power and its corresponding receiver position is called a training point. The positioning accuracy improves as the number of training points increases. For larger environments, building the power map becomes a cumbersome task. In order to reduce the number of training points required to achieve a certain positioning accuracy, some methods rely on logarithmic interpolation [17]. However, the layout of a real indoor environment could introduce discontinuities in the power map, rendering interpolation methods inefficient. Fig. 2 illustrates how discontinuities in the power map are created. The measured received power at position $p_1$ is $P_r(d)$, and the measured received power at position $p_2$ is $P_r(d) + L_p$. Although $p_1$ and $p_2$ are spatially close and are at the same distance $d$ from the transmitter, the corresponding received powers are not equal. Subsequently, the distance estimate based on $P_r(d)$ will be close to $d$, whereas the distance estimate based on $P_r(d) + L_p$ will be different from $d$, i.e. close to $d'$, and the receiver could be therefore estimated to be at position ${p'}_2$.

An intermediary approach that mitigates interpolation inaccuracies while minimizing the number of required training points is proposed. This approach relies on "strategically" subdividing the indoor environment into small areas, or clusters, where the received power at any point in a given cluster can be accurately interpolated. The size and shape of the clusters is dictated by the geometry of the

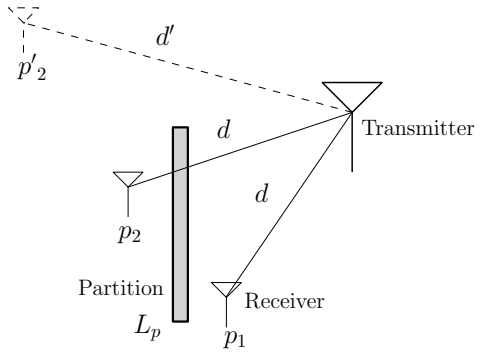


Fig. 2. Distance estimation error in the presence of a partition with an attenuation loss $L_p$. The antenna of the transmitter is assumed to be isotropic. If the receiver is at $p_2$, the estimated position could be at $p'_2$.

environment. It suffices to collect one training point– or reference point, from each cluster to build the power map with a certain level of accuracy. Determining the boundaries of the clusters is discussed in subsection III-A.1, and building the power map is discussed in subsection .

### A.1 Obtaining Cluster Boundaries

In order to determine the boundaries of the clusters, the layout of the indoor environment and the transmitter locations must be known. Furthermore, it is assumed that the fixed partitions are the only source of obstructions between the transmitter and the receiver.

The first step of the clustering algorithm is to generate a uniform grid of points that will constitute the power map. It is assumed that the receiver height is known and constant. It is therefore sufficient to build a 2-dimensional power map covering the $xy$-plane of the environment. The grid spacing $\Delta s$ is uniform and equal in both the $x$ and $y$ direction. Next, each distinct wall and floor material is assigned a material identifier (MID). The MID of all the wall and floor partitions obstructing the LOS between any point and a given transmitter $j$ are stored as an attribute in the column vector $\boldsymbol{m}_p^{(j)}$ of size $M$, where $M$ is the total number of distinct MIDs. Each element $m_p^{(j)}(i)$ in $\boldsymbol{m}_p^{(j)}$ holds the number of obstructing walls having a MID $i$, with $i \in \{1, 2, 3, ..., M\}$. For example, if only walls are considered as the source of obstruction, $\boldsymbol{m}_p^{(1)} = [3, 0, 2]$ indicates that three walls of MID=1, no walls of MID=2, and two walls of MID=3 are obstructing transmitter 1.

For any point $p$, the MID matrix $\boldsymbol{M}_p$ is defined as $\boldsymbol{M}_p \triangleq [\boldsymbol{m}_p^{(1)}, \boldsymbol{m}_p^{(2)}, ..., \boldsymbol{m}_p^{(N_T)}]$. A cluster $C_l$ is defined as the cluster of adjacent points having the same MID matrix. The steps of the clustering algorithm are illustrated in Fig. 3. In this example, the indoor environment is assumed to have one wall partition with MID=1, two transmitters, and $M = 2$, as depicted in Fig. 3a). The cluster of points in the LOS of Transmitter 1, corresponding to the white area in Fig. 3b), will have a MID vector $\boldsymbol{m}_p = (\,0\;0\,)$, and the cluster of points in the NLOS or shaded are will have a MID vector $\boldsymbol{m}_p = (\,1\;0\,)$. It is clear that the same MID vectors will be obtained in the white and shaded areas of Fig. 3c) for Transmitter 2. Three different MID matrices are constructed from the $\boldsymbol{m}_p$ vectors, with $\boldsymbol{M}_p = \left(\begin{smallmatrix}0&0\\0&0\end{smallmatrix}\right)$ beign associated with the points in $C_3$ and $C_4$, $\boldsymbol{M}_p = \left(\begin{smallmatrix}0&0\\1&0\end{smallmatrix}\right)$ with $C_1$, and $\boldsymbol{M}_p = \left(\begin{smallmatrix}1&0\\0&0\end{smallmatrix}\right)$ with $C_2$. Since $C_3$ and $C_4$ are not spatially adjacent, they are not combined together and therefore a total of four clusters are obtained, as shown in Fig. 3d).

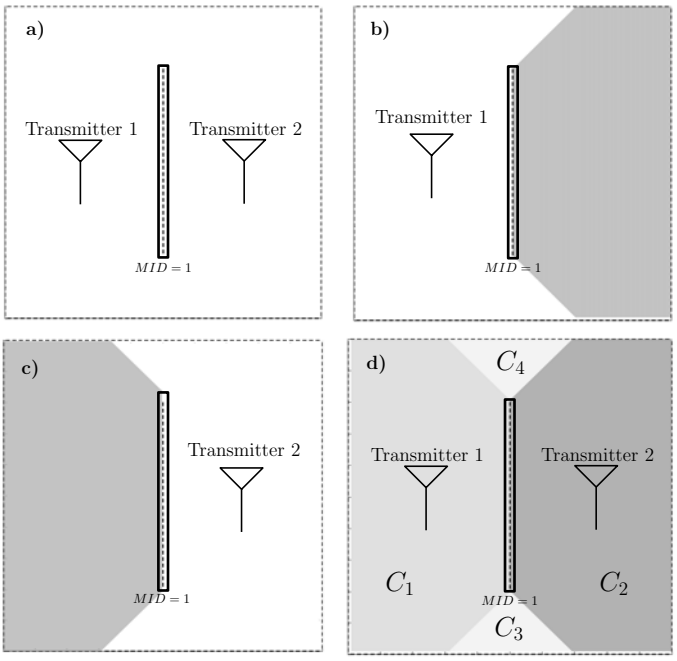


Fig. 3. Clustering example with 2 transmitters, 1 partition (MID=1) and M=2. a) Environment layout, b) Clustered areas with respect to Transmitter 1, c) Clustered areas with respect to Transmitter 2, and d) Resulting cluster map for the entire environment and both transmitters. The colors are used only to distinguish between different clusters.

It is denoted by $C_l$ any cluster $l$, with $l \in \{1, 2, 3..., N_C\}$, where $N_C$ is the total number of clusters, which is a function $N_w$, $N_f$, $N_T$, and $\Delta s$. Since indoor environments are not identical, no simple or straightforward analytical relation between $N_C$, $N_w$, $N_f$, $N_T$, and $\Delta s$ can be derived. Fig. 4 shows simulation plots for the total number of cluster $N_C$ as a function of the number of transmitters, the number of partitions in the environment, and the grid spacing. In Fig. 4, $N_w$ and $N_f$ are combined into one term $N_P$, which is defined as the total number of partitions. As expected, $N_C$ increases when $N_P$ and/or $N_T$ increase and/or when $\Delta s$ decreases.

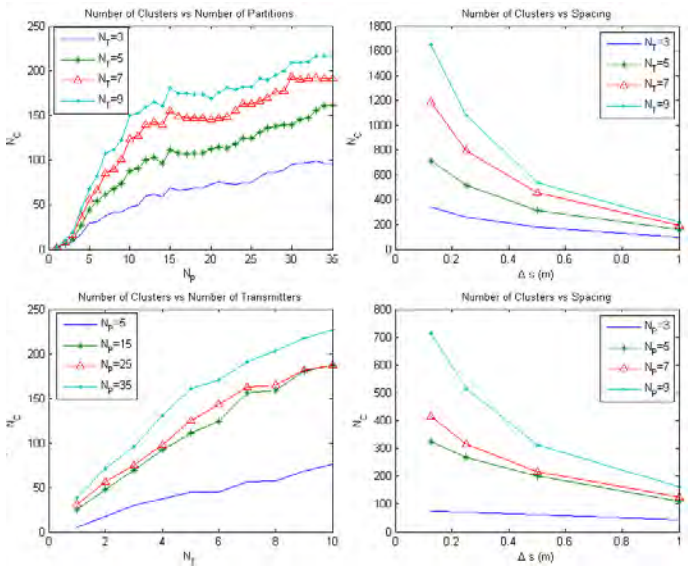


Fig. 4. Variation of the number of clusters with respect to the number of partitions $N_P$, number of transmitters $N_T$, and grid spacing $\Delta s$.

### A.2 Building the Power Map

Only one reference point from each cluster $C_l$ is needed to build the entire power map. The power received at the reference point in cluster $l$ is given by

$$P_{r_l}^{(j)}(d,\phi,\theta) = P_0^{(j)} - 10\,n\,\log_{10}\left(\frac{d_l^{(j)}}{d_0^{(j)}}\right) + L_{p_l}^{(j)} + L_{D_l}^{(j)}(\phi,\theta),$$

where $P_{r_l}^{(j)}(d_l,\phi,\theta)$ is the measured received power at the reference point in cluster $C_l$ and at a distance $d_l^{(j)}$ from transmitter $j$ and $L_{p_l}^{(j)}$ is the total losses due to partitions obstructing transmitter $j$ from cluster $l$. Since $P_{r_l}^{(j)}(d,\phi,\theta)$, $d_l^{(j)}$, $P_0^{(j)}$ and $d_0^{(j)}$ are known and $L_{D_l}^{(j)}(\phi,\theta)$ can be extracted from the radiation pattern of the transmitting antenna, $L_{p_l}^{(j)}$ can be calculated from

$$L_{p_l}^{(j)} = P_0^{(j)} - 10\,n\,\log_{10}\left(\frac{d_l^{(j)}}{d_0^{(j)}}\right) + L_{D_l}^{(j)}(\phi,\theta) + P_{r_l}^{(j)}(d,\phi,\theta).$$

For any given cluster $C_l$, the partition losses $L_{p_l}^{(j)}$ at any point in $C_l$ are constant. Therefore, the received power at any point in any cluster $C_l$ can be calculated using (4).

## B. VLOS Positioning Algorithm

The positioning proposed algorithm relies on correcting the measured received power for partition and angle losses. A position estimate of the receiver is required to calculate these losses. The MM algorithm used to determine the position estimate is discussed in the following subsection. Finally, the EKF used to fuse the MM position estimate with the distances calculated from the VLOS power is discussed.

### B.1 VLOS Map-Matching Algorithm

An initial estimate for the receiver's position is produced using the power map generated in the offline stage. The VLOS-MM algorithm operates according to the following steps

- Define $\mathcal{P} \triangleq \{p_1, p_2, ..., p_{N_\alpha}\}$ as the set of points of cardinality $N_\alpha$ such that every point $p_i \in \mathcal{P}$ satisfies the condition:

$$||P_r(p_{rx}) - P_r(p_i)||_2 < \alpha,$$

where $P_r(p_{rx}) = [P_r^{(1)}(p_{rx}), ..., P_r^{(N_T)}(p_{rx})]^T$ is the vector of measured received powers from each transmitter at the receiver position, $P_r(p_i) = [P_r^{(1)}(p_i), ..., P_r^{(N_T)}(p_i)]^T$ is the vector of received powers from each transmitter at position $p_i$ that is extracted from the power map, and $\alpha$ is a tolerance threshold tuned by trial and error (typically between 6 and 12).
- Assuming that the receiver is in cluster $\mathcal{C}$, then $\mathcal{C} \triangleq \max_l \{\text{card}\,(\mathcal{P} \cap C_l)\}$ where $C_l$ is cluster $l$ with $l \in \{1, 2, 3, ..., N_C\}$.
- Define the set of points $\wp \triangleq \mathcal{P} \cap \mathcal{C}$.
- The MM position estimate $\hat{p}$ is then calculated as the average of the set of points $\wp$.

The partition losses $L_p$ and angle losses $L_D(\phi_{\hat{p}}, \theta_{\hat{p}})$ pertaining to the MM estimate of the receiver position $\hat{p}$ are then calculated. The measured received power is corrected according to (5). The distance from the transmitter is deduced from the VLOS power and passed as an observation to an EKF discussed next.

### B.2 Extended Kalman Filter Model

In this paper, the receiver is assumed to be stationary, therefore, the position of the receiver has the dynamics

$$\boldsymbol{x}_r(k+1) = \boldsymbol{x}_r(k), \qquad k = 1, 2, 3, ... \tag{8}$$

where $\boldsymbol{x}_r(k) = (x(k), y(k))^T$ is the position state of the receiver. Two sets of observations are passed to the EKF: (1) the initial position of the receiver extracted from the MM algorithm and (2) the distances extracted from the VLOS power. Therefore, the EKF assumes the following observation model

$$\rho^{(j)}(k) = \sqrt{(x(k) - x^{(j)})^2 + (y(k) - y^{(j)})^2} + v^{(j)}(k)$$
$$\boldsymbol{\rho}_{MM}(k) = \boldsymbol{x}_r + \boldsymbol{v}_{MM}(k), \tag{9}$$

where $x^{(j)}$ and $y^{(j)}$ are the coordinates of transmitter $j$, $\rho^{(j)}(k)$ is the observed distance between transmitter $j$ and the receiver calculated from the VLOS power, and $\boldsymbol{\rho}_{MM}(k)$ is the position estimate obtained by the MM algorithm. The noise terms $v^{(j)}(k)$ are independent and their statistics are described in II-B, and the noise term $\boldsymbol{v}_{MM}(k)$ is a zero-mean Gaussian random variable with a covariance matrix $\boldsymbol{R} = r_{xy}\,\boldsymbol{I}$. The Jacobian is given by

$$\boldsymbol{H} = \begin{pmatrix} \frac{x-x^{(1)}}{\sqrt{(x-x^{(1)})^2+(y-y^{(1)})^2}} & \frac{y-y^{(1)}}{\sqrt{(x-x^{(1)})^2+(y-y^{(1)})^2}} \\ \frac{x(k)-x^{(2)}}{\sqrt{(x-x^{(2)})^2+(y-y^{(2)})^2}} & \frac{y-y^{(2)}}{\sqrt{(x-x^{(2)})^2+(y-y^{(2)})^2}} \\ \vdots & \vdots \\ \frac{x-x^{(N_T)}}{\sqrt{(x-x^{(N_T)})^2+(y-y^{(N_T)})^2}} & \frac{y-y^{(N_T)}}{\sqrt{(x-x^{(N_T)})^2+(y-y^{(N_T)})^2}} \\ 1 & 0 \\ 0 & 1 \end{pmatrix}$$

At each time step k, the position estimate produced by the MM algorithm and the distances calculated from the VLOS power are passed as new measurements to the EKF. The VLOS indoor localization algorithm described in sections II and III is summarized in the flowchart illustrated in Fig. 5.

## IV. SIMULATION AND EXPERIMENTAL RESULTS

In this section, the simulation and experimental results for the proposed positioning algorithm are presented. The experiments were conducted in the west wing of the third floor of Winston Chung Hall in The University of California, Riverside. The part of the floor considered for the experiments consists of research laboratories and has a total of 35 wall partitions. Four transmitters are employed for VLOS positioning. The layout of the environment is shown in Fig. 6.

The grey shaded areas are excluded from the test environment. Transmitters 1, 2 and 3 are CISCO 3700i APs mounted on the ceiling with $P_0 = -5$ dBm and $d_0 = 2.664$ m each. The radiation pattern of the antennas of these transmitters is illustrated in Fig 1. Each of these three transmitters has three different antennas transmitting at the same time. The actual power received is assumed to be the average of the individual power received from each of the three antennas. Transmitter 4 is a standard TP-Link TL-WR841N home router with $P_0 = -12$ dBm and $d_0 = 2.664$ m. The radiation pattern of Transmitter 4 in the azimuth plane is assumed to be uniform. No losses due to the elevation angle are considered, since the router has been placed at the receiver's height. A total of seven MIDs representing glass, birck, concrete, soft partition (gypsum), double soft partition, ceramic tiles and thick fabric materials, all of which are present in the selected environment, were considered for the simulations and the experiments.

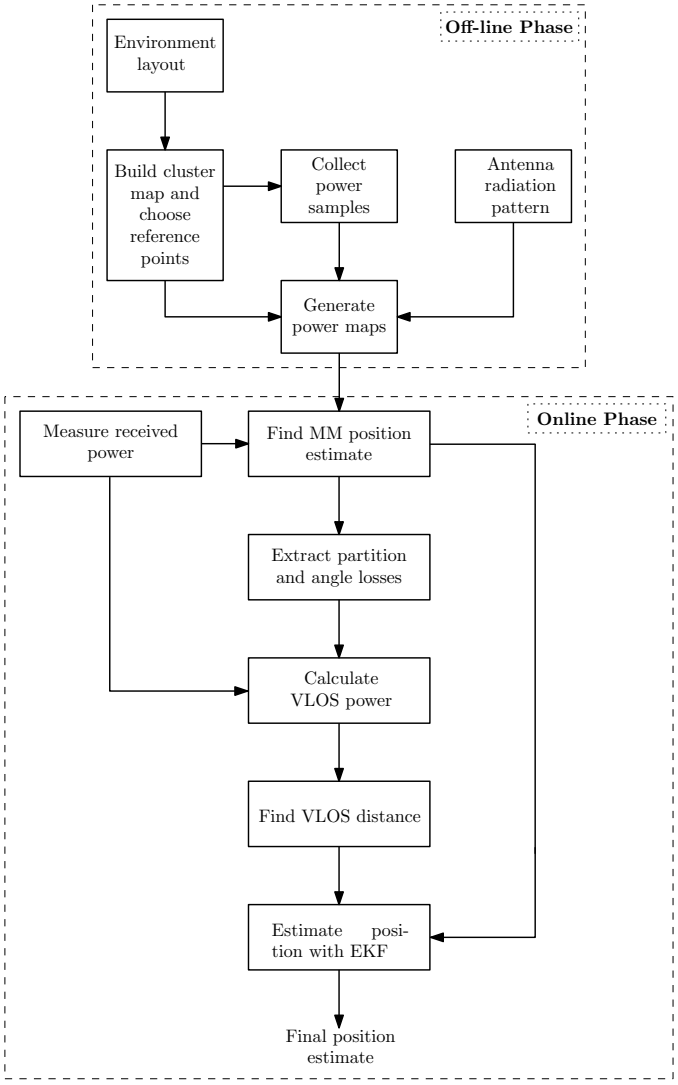


Fig. 5. Indoor VLOS localization flowchart.

### A. Map Building

The first phase of the VLOS positioning algorithm is to build the power map off-line. This is achieved by first clustering the space and then collecting the training points. The clustering algorithm proposed in III-A.1 is applied to the test environment, with $\Delta s = 0.125$ m, resulting with the cluster map shown in Fig. 7. With $N_T = 4$, $N_P = 35$ and $\Delta s = 0.125$ m, the total number of clusters in Fig. 7 was $N_C = 225$. The reference received powers were sampled at the center of each cluster and at a constant height of 0.736 m, which is assumed to be the height of the receiver. The received power maps were generated using these training points, as discussed in subsection III-A.2. Fig. 8 shows the power map pertaining to each of the four transmitters.

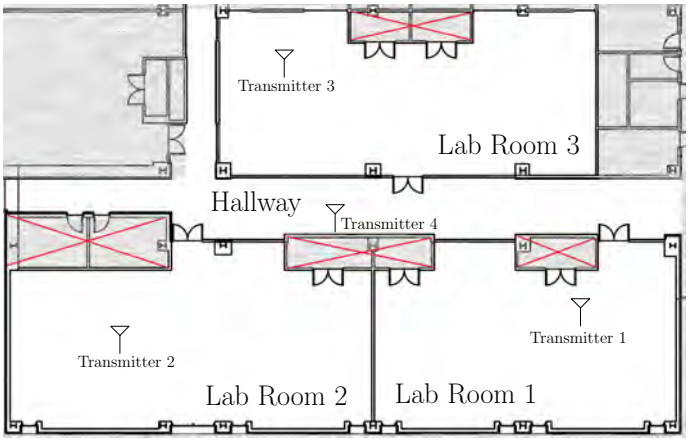


Fig. 6. Layout of the test environment at the third floor of Winston Chung Hall in The University of California, Riverside.

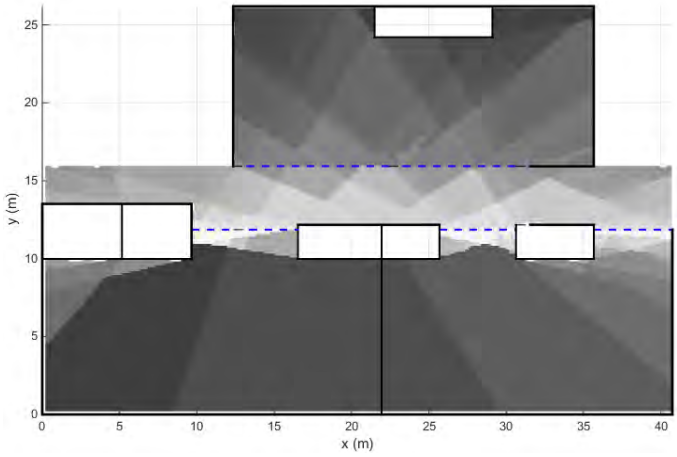


Fig. 7. Cluster map of the environment. The colors are only used to distinguish between different clusters.

## B. VLOS Positioning Results

The VLOS-MM with the EKF and VLOS-MM alone algorithms were tested. Several receiver positions were considered, as shown in Fig. 9.

To compute the received power noise standard deviation $\sigma$, power samples across different days and for several hours were collected, yielding $\sigma = 2.36$ dB. This is a relatively high noise standard deviation, which is due to the test environment in Winston Chung Hall being designed as a semi-indoor environment in which the corridors are actually outdoors and the laboratories indoors; hence containing brick walls, metallic rails, etc.

The simulation and experimental positioning errors for VLOS-MM-EKF and VLOS-MM alone are shown in Fig. 10 and Fig. 11 respectively. The plots show the mean positioning error and its corresponding standard deviation for VLOS positioning, for two, three and four transmitters. It is assumed that the path exponent $n = 2$. The tolerance

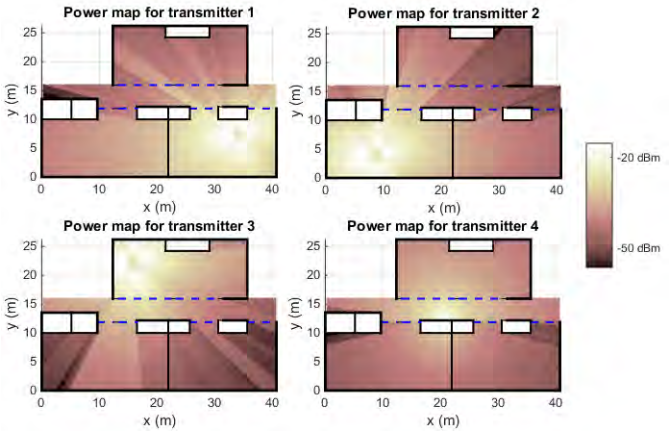


Fig. 8. Power maps for transmitters 1, 2, 3 and 4.

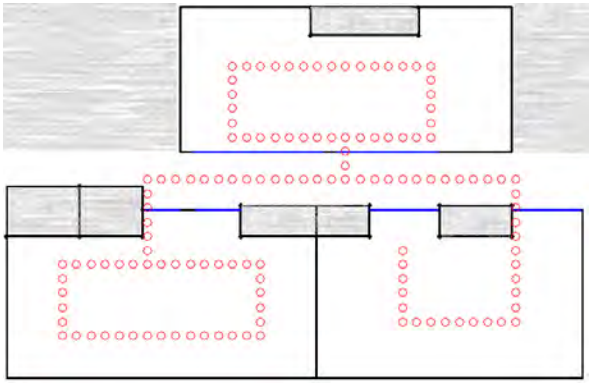

Fig. 9. Receiver positions considered for the experiment (red circles).

threshold $\alpha$ was chosen to be 10.4 dB.

It can be seen from Fig. 10 and Fig. 11. that the simulation and experimental results match well. Furthermore, it can be deduced that VLOS-MM-EKF performs better than VLOS-MM alone. In real applications, more than three transmitters are used for positioning. In the case of four transmitters, the error and standard deviation are 2.58 m and 1.61 m respectively for simulated VLOS-MM-EKF positioning, and 2.49 m and 1.63 m experimentally. The experimental results for three and four transmitters are summarized in Table I and Table II, respectively, including the kNN solution using the same training points.

TABLE I
MEAN ERROR (ME) AND STANDARD DEVIATION (STD) OF EXPERIMENTAL POSITIONING RESULTS FOR THREE TRANSMITTERS.

| **Algorithm** | **ME (m)** | **StD (m)** |
|---|---|---|
| VLOS-MM-EKF | 3.19 | 1.98 |
| VLOS-MM | 3.55 | 2.58 |
| kNN | 5.54 | 3.43 |

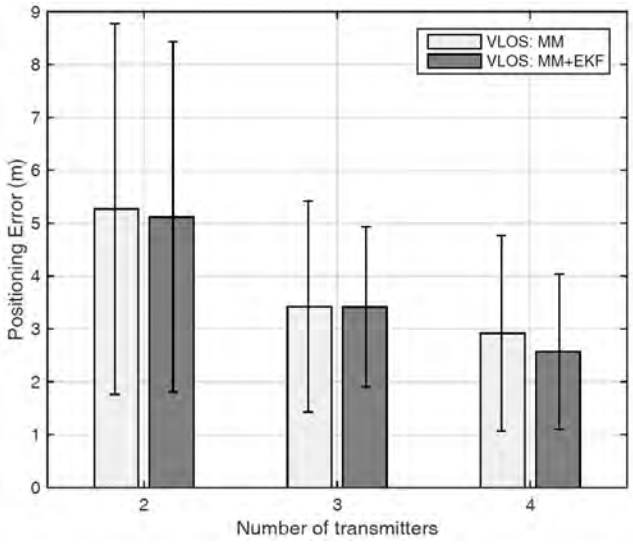


Fig. 10. Simulation mean error (bars) and standard deviation (error bars) for two, three and four transmitters. $\sigma = 2.36$ dB.

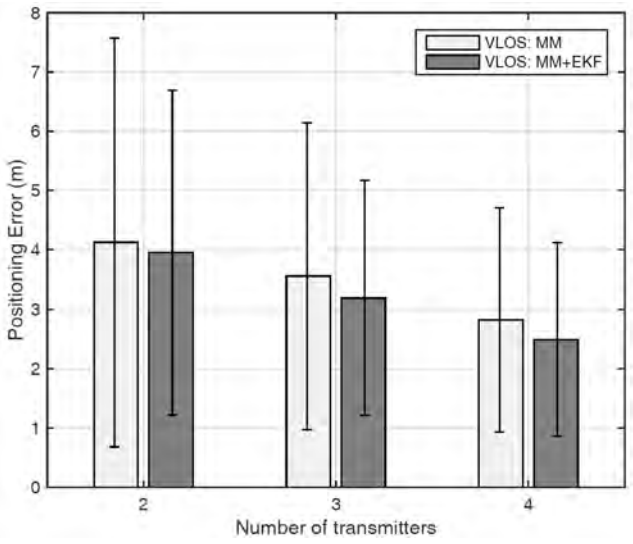


Fig. 11. Experimental mean error (bars) and standard deviation (error bars) for two, three and four transmitters. $\sigma = 2.36$ dB.

TABLE II
MEAN ERROR (ME) AND STANDARD DEVIATION (STD) OF EXPERIMENTAL POSITIONING RESULTS FOR FOUR TRANSMITTERS.

| **Algorithm** | **ME (m)** | **StD (m)** |
|---|---|---|
| VLOS-MM-EKF | 2.49 | 1.63 |
| VLOS-MM | 2.82 | 1.84 |
| kNN | 4.87 | 2.82 |

It can be seen from Table I and Table II that for three or more transmitters, VLOS positioning outperforms kNN, with VLOS-MM-EKF performing better than VLOS-MM alone. The training points sampled for building the power map can be up to meters apart, which makes the kNN algorithm perform poorly. However, using the VLOS algorithm, the same training points are used to build a more accurate power map with an arbitrarily small grid spacing $\Delta s$, which means that more neighbors will have similar power to the measured power, hence a more accurate position estimate. It is worth mentioning that the proposed VLOS algorithm is expected to provide higher levels of accuracy in truly indoor environments with lower $\sigma$. Fig. 12 shows the simulation results for the map matching solution and the VLOS positioning algorithm for $\sigma = 1.2$ dB. It can be seen that the positioning error becomes at the submeter level, with a VLOS positioning mean error of 0.462 m and a standard deviation of 0.367 m.

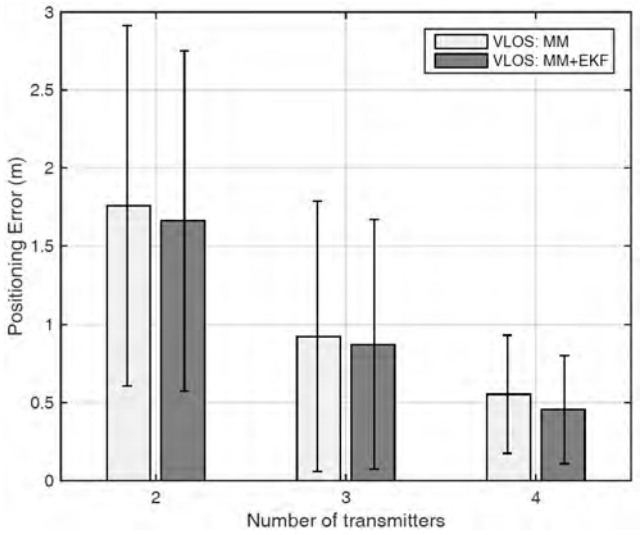


Fig. 12. Simulation mean error (bars) and standard deviation (error bars) for two, three and four transmitters. $\sigma = 1.2$ dB.

## V. Conclusion

In this paper, an indoor positioning algorithm relying on RSSI was proposed. To this end, an efficient power map building approach that exploits the layout of the indoor environment was developed and a positioning algorithm that is based on correcting the received power for the partitioning and obstacle losses present in the environment was proposed. An initial position estimate that is solely based on map matching is first produced, and the partition losses associated with this position are then calculated. Once the received power is corrected, the distances from the receiver to the transmitters are calculated and passed as observations along with the position estimate obtained by map-matching to an EKF. The EKF fuses these observations and produces a final position estimate for the receiver. The VLOS positioning algorithm has been simulated and experimentally tested for a semi-indoor environ-

ment. The experimental and numerical results matched well. VLOS positioning performed well in the presence of high noise. Simulations for an environment with a lower noise standard deviation shows that VLOS positioning improves the positioning accuracy to the submeter level, with an average positioning error of less than half a meter.

The proposed future work includes improving the map building approach by requiring less points without sacrificing the accuracy. Furthermore, analytical expressions for the mean and covariance of the noise associated with the initial position estimate obtained by map matching could be derived. Finally, further experimental work should be conducted, especially in less noisy environments, to validate the simulation results presented in Fig. 12.

## References


[1] H. Liu, H. Darabi, P. Banerjee, and J. Liu, "Survey of wireless indoor positioning techniques and systems," *IEEE Transactions on Systems, Man, and Cybernetics–Part C*, vol. 37, no. 6, pp. 1067–1080, Nov. 2007.

[2] Y. Gu, A. Lo, and I. Niemegeers, "A survey of indoor positioning systems for wireless personal networks," *IEEE Communications Surveys & Tutorials*, vol. 11, no. 1, pp. 13–32, Nov. 2009.

[3] Y. Zhuang, Z. Shen, Z. Syed, J. Georgy, H. Syed, and N. El-Sheimy, "Autonomous WLAN heading and position for smartphones," in *Proc. IEEE/ION Position, Location and Navigation Symposium - PLANS*, May 2014, pp. 1113–1121.

[4] S. Kumar, S. Gil, D. Katabi, and D. Rus, "Accurate indoor localization with zero start-up cost," in *Proc. of international conference on Mobile computing and networking*, Sep. 2014, pp. 483–494.

[5] C. Serodio, L. Coutinho, and L. Reigoto, "A lightweight indoor localization model based on Motley-Keenan and COST," in *Proc. World Congress on Engineering*, vol. 2, Jul. 2012, pp. 1–6.

[6] G. Ding, Z. Tan, J. Zhang, and L. Zhang, "Regional propagation model based fingerprinting localization in indoor environments," in *Proc. International Symposium IEEE Personal Indoor and Mobile Radio Communications (PIMRC)*, Sep. 2013, pp. 291–295.

[7] X. Zhang, Y. Jin, H. Tan, and W. Soh, "CIMLoc: A crowdsourcing indoor digital map construction system for localization," in *Proc. IEEE International Conference on Intelligent Sensors, Sensor Networks and Information Processing (ISSNIP)*, Apr. 2014, pp. 1–6.

[8] Y. Lee and S. Park, "RSSI-based fingerprint map building for indoor localization," in *Proc. of International Conference on Robotics and Ambient Intelligence*, Oct. 2013, pp. 292–293.

[9] J. Liao, Z. Zhou, G. Tsai, T. Duong, and K. Chiang, "The applicability analysis of using smart phones for indoor mobile mapping applications," in *Proc. of ION GNSS*, Sep. 2014, pp. 510–531.

[10] V. Moghtadaiee and A. Dempster, "Indoor location fingerprinting using FM radio signals," *IEEE Transactions on Broadcasting*, vol. 60, no. 2, pp. 336–346, Jun. 2014.

[11] G. Chen, Y. Zhang, L. Xiao, J. Li, L. Zhou, and S. Zhou, "Measurement-based RSS-multipath neural network indoor positioning technique," in *Proc. IEEE Canadian Conference on Electrical and Computer Engineering (CCECE)*, May 2014, pp. 1–7.

[12] M. Zhou, Q. Zhang, Z. Tian, F. Qiu, and Q. Wu, "Correlated received signal strength correction for radio-map based indoor Wi-Fi localization," in *Proc. of International Conference on Computing, Communications and Networking Technologies*, Jul. 2014, pp. 1–6.

[13] R. Faragher and R. Harle, "An analysis of the accuracy of Bluetooth low energy for indoor positioning applications," in *Proc. of ION GNSS*, Sep. 2014, pp. 201–210.

[14] S. Ali-Loytty, T. Perala, V. Honkavirta, and R. Piche, "Fingerprint Kalman filter in indoor positioning applications," in *Proc. of IEEE International Conference on Control Applications*, Jul. 2009, pp. 1678–1683.

[15] P. Anindya and W. Eric, "Wi-Fi based indoor localization and tracking using sigma-point Kalman filtering methods," in *Proc. IEEE/ION Position, Location and Navigation Symposium*, May 2008, pp. 646–659.

[16] X. Chen, J. Kong, Y. Guo, and X. Chen, "An empirical study of indoor localization algorithms with densely deployed APs," in *Proc. IEEE Global Communications Conference (GLOBECOM)*, Dec. 2014, pp. 517–522.

[17] Y. Liu and S. Jan, "Assessment of indoor positioning system using Kriging fingerprinting method and IEEE 802.11v standard," in *Proc. of ION GNSS*, Sep. 2014, pp. 1622–1628.

[18] S. Saab and Z. Kassas, "Power matching approach for GPS coverage extension," *IEEE Transactions on Intelligent Transportation Systems*, vol. 7, no. 2, pp. 156–166, Jun. 2006.

[19] T. Rappaport, *Wireless Communications: Principles and Practice*, 2nd ed. Upper Saddle River: Prentice Hall, 2002, ch. 4 Mobile Radio Propagation: Large-Scale Path Loss.

[20] CISCO Systems, Inc., "Cisco Aironet Series 1700/2700/3700 Access Points Deployment Guide," http://www.cisco.com/c/en/us/td/docs/wireless/technology/apdeploy/8-0/Cisco_Aironet_3700AP.html, 2014, accessed April 19, 2015.